communications earth & environment

ARTICLE

https://doi.org/10.1038/s43247-022-00602-7 OPEN

Chemical weathering over hundreds of millions of years of greenhouse conditions on Mars

Binlong Ye [1] & Joseph R. Michalski [1✉]

Chemical weathering profiles on Mars which consist of an upper Al clay-rich, Fe-poor layer and lower Fe/Mg clay-rich layer are believed to have formed due to precipitation-driven top down leaching process in an ancient, reducing greenhouse climate. Here we use remote sensing imagery and spectroscopy coupled with topographic data and crater chronology to explore the geological characteristics, stratigraphy and relative age of >200 weathering profiles across the southern highlands of Mars. We find that nearly all exposures show a similar, single stratigraphic relationship of Al/Si materials over Fe/Mg clays rather than multiple, interbedded mineralogical transitions. This suggests either one single climate warming event or, perhaps more likely, chemical resetting of weathering horizons during multiple events. While the time required to form a typical martian weathering profile may have been only ~10^6–10^7 years, the profiles occur in deposits dating from the Early Noachian into the Hesperian and suggest that chemical weathering may have occurred over a large range of geologic time, with a peak around 3.7–3.8 billion years ago.

[1] Department of Earth Sciences, University of Hong Kong, Hong Kong, China. ✉email: jmichal@hku.hk

The surface of Mars is desiccated, cold, and oxidized today. However, ancient parts of the crust contain hundreds of channel networks and dry lakes that must have formed in a warmer and wetter climate of the modern environment[1,2]. Theoretical modeling of the conditions and mechanisms of past climate warming has presented a major challenge to scientists. Though the enigma of past climate change on Mars is far from answered, several pieces of the puzzle are now better resolved. Most plausible explanations for a wetter ancient climate involve strong greenhouse warming of a thicker early atmosphere[3–5] driven by reducing greenhouse gas, such as H_2 and CH_4 mixed with other gases, including CO_2[4,6–9]. Geological uncertainties surrounding ancient climate include the question of whether climate changed in one major warming event[5,10,11] or whether multiple or many cycles of episodic warming and cooling occurred in the Noachian. Another question is whether the climate was truly warm globally or if significant regional variations might have occurred. A complex model was put forward to link redox cycles with climate cycles on Mars, posing the question of whether Mars oscillated between a warm reducing and colder oxidizing atmospheric state[9].

Further clues to ancient climate include hydrated alteration minerals that formed by a reaction between the silicate crust with surface water, atmosphere, aerosols, and possibly snow or ice. On Earth, weathering profiles, or the chemical-mineralogical-textural alteration fronts affecting rocks and particulate matter at the surface trace modern chemical weathering and paleo-weathering. During weathering, chemical changes caused by top-down leaching processes are driven by the acids and oxidants in the atmosphere-lithosphere interface. Ca, Mg, Na, K, and Mn are considered as mobile elements, while Ti, Al, and Zr are essentially immobile. The loss of mobile elements and retention of immobile elements leads to significant differences in soil profiles[12,13]. This concept has been applied to Mars, where exposures of compositional stratigraphy, consisting of an upper Al clay-rich layer and a lower Fe/Mg smectite layer, have been interpreted as paleo-weathering profiles[14–17]. Paleo-weathering profiles are not only evidence for water–rock interaction, but also serve as an indicator of redox conditions. Under reducing conditions, Fe occurs in its soluble ferrous form and the process of chemical weathering usually leaches Fe^{2+} [12]. Tracking of Fe-mobility is therefore a tool to understand both climate and redox state on early Mars at the same time. Recent work showing evidence of Fe-mobility in weathering profiles suggests past climate warming occurred under reducing conditions[18].

The southern highlands of Mars contain many exposures of candidate weathering deposits where Fe/Mg smectites are overlain by Al/Si materials. Most of them have not been studied in considerable detail, and questions regarding the climatic evolution of Mars remain: (1) Are these weathering events local or global? (2) Do we see multiple events preserved in the same stratigraphy, or does each deposit record only one event? (3) What are the ages of the different exposures? Could they plausibly all represent the same geologic/climate episode, or are they indicative of different climate excursions at different times? (4) Could the age, distribution, and style of the chemical weathering deposits/relationships constrain the climate warming mechanism?

Here, we carried out a global analysis of 203 exposures of compositional stratigraphy, consisting of Al/Si materials and Fe/Mg smectites, in order to present a comprehensive picture of evidence for paleo-weathering and implications for climate. Building upon multiple prior studies[14,15,19–41], we analyzed 54 additional deposits, and revisited previously reported sites in order to provide several additional key observations about global weathering, constraining climate, and redox evolution recorded in these critical ancient geological deposits.

Results

Geological characteristics of compositional stratigraphy. Over 203 compositional deposits, consisting of Al clays and Fe/Mg smectites, across the surface of Mars were evaluated, including 54 new detections in this study (Fig. 1). Most of them were found in Mawrth Vallis, Eridania northern basin, Valles Marineris, Nili Fossae, Simois colles/Gorgonum chaos, Noachis Terra and Hellas Basin (Fig. 1a). The latitude distribution of these sequences is mainly within the range from 40 °S to 30 °N, although it may be affected by the modern polar process that have physically obliterated or spectrally obfuscated the deposits. This latitude distribution of weathering sequences is similar to the distribution of other relevant geologic features such as valley networks and open basin lakes[42–44] (Supplementary Fig. 1). Latitude-dependence of compositional stratigraphy could be consistent with a "tropical" control on precipitation patterns. They show considerable variation in elevation from −3000 to 6000 m (Fig. 1b). Nearly 88% of these exposures occur in Noachian terrain units[45]. Specifically, 65 locations occur in the early Noachian units (Early Noachian highland unit and Early Noachian highland massif unit), 85 in the middle Noachian units (Middle Noachian highland unit and Middle Noachian highland massif unit), 28 in the Late Noachian units (Late Noachian highland unit), and 18 in the Hesperian and Noachian transition units (Fig. 1c). Based on generalized crater age dating of these map units where the paleo-weathering sequences occur, as well as counting carried out in this study, the oldest weathering profiles occur in rocks as old as 3.97 Ga and as young as 3.18 Ga.

The exposures of compositional stratigraphy were identified in a wide spectrum of geologic contexts (Fig. 2), including impact crater floors, crater rims, crater walls, intercrater plains and basins, within valley networks, and knobby terrain of Eridania of deep basin deposits. Remote sensing identification of paleo-weathering profiles is unfortunately affected by observational biases. Compositional stratigraphy is easiest to identify in high slopes within low-dust regions, such as within massifs, knobs, volcanic edifices, erosional windows, and crater rims. It is very likely that compositional stratigraphy is much more extensive than what the exposed, detectable evidence suggests.

In addition, we have examined over 154 weathering deposits with HiRISE color images with a submeter spatial resolution. Previous studies have shown that color patterns in HiRISE IRB (infrared, red, and green-blue) images can be used synergistically with CRISM data to reveal higher-resolution views of compositional relations and to extrapolate from areas where CRISM data exist to areas where only HiRISE data exist[18]. This is possible because the weathering profiles are typified by a blue-toned unit overlying red, brown, yellow color units wavelength of HiRISE color image, due to the relative abundance of the main pigment Fe^{3+} in the rocks[18]. The white/bluish unit usually corresponds to the unit rich in Al clay minerals as seen with OMEGA and CRISM while the red/brown unit represents the Fe/Mg smectites (Fig. 2).

HiRISE color images not only provide a proxy for mapping compositional units at a higher resolution but also reveal the characteristics of contacts between upper and lower units. The transition of these two colors in HiRISE images, from white to red, is generally gradual, not sharp. The compositional layering does not follow bedding planes and therefore the compositional units appear to exhibit inherited textures and fabric from the units in which the alteration occurs. These patterns have been interpreted as the evidence of Fe loss in reduced conditions[18]. If compositional stratigraphy is indeed linked to Fe mobility, then our results demonstrate that strong Fe loss was a widespread process affecting much of the southern highlands of Mars.

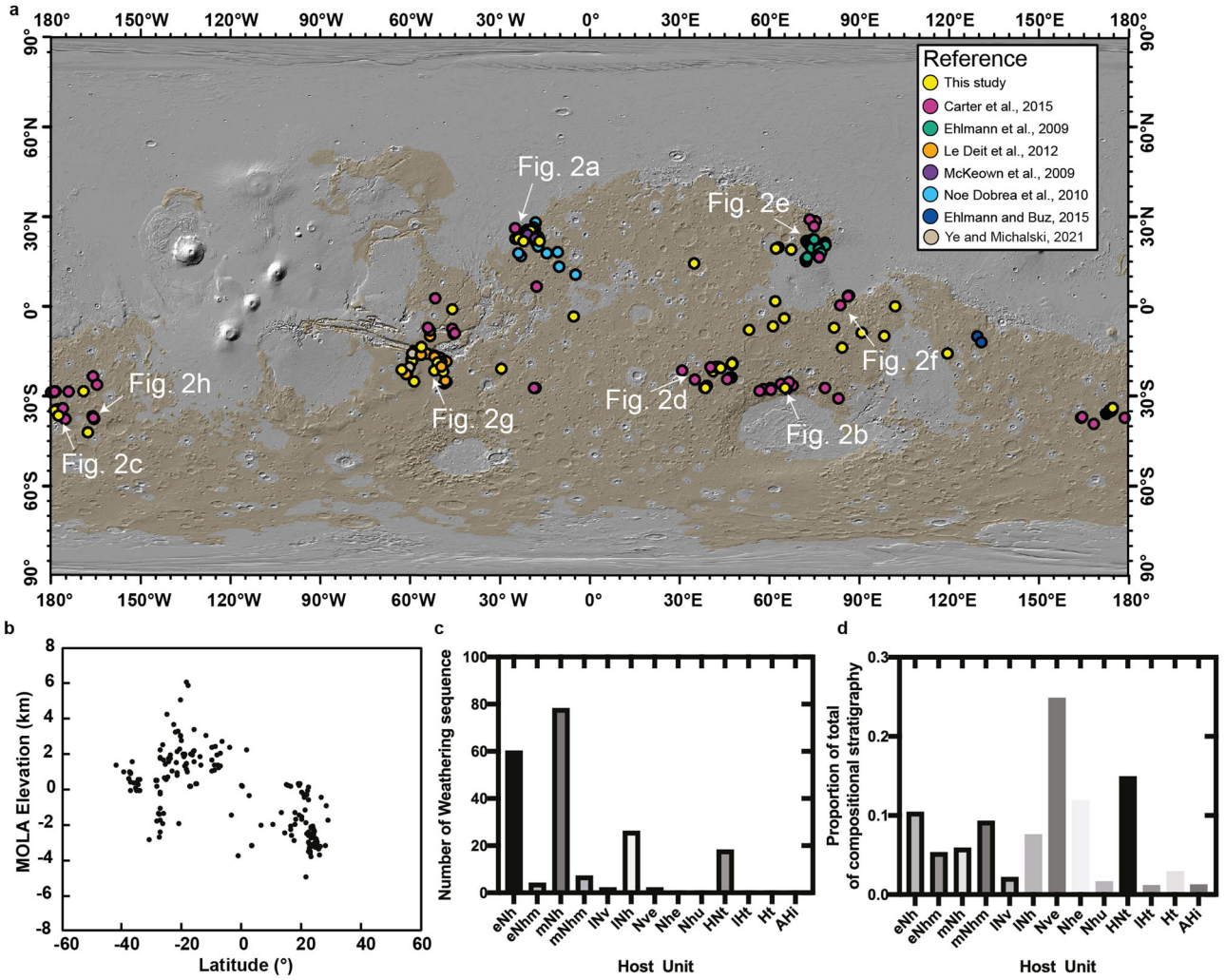

Fig. 1 Compositional stratigraphy deposits on Mars, consisting of Al/Si materials and Fe/Mg smectites. a This global map shows the locations of 203 outcrops of compositional stratigraphy on Mars including those compiled from previous studies and 54 new detections presented in this work (Supplementary Table 1). The different colors indicate 203 exposures of compositional stratigraphy compiled from the previous studies[14,15,19–41] and 54 additional new detections in this contribution (Supplementary Table 1). The based map is Mars Orbiter Laser Altimeter hillshade data (gray) drapped by Noachian geology units (brown)[45]. **b** Analysis of the latitude and MOLA elevation of 203 compositional exposures show a wide range of elevations and confined latitudes of these deposits. **c** A histogram of the host unit for compositional stratigraphy shows the range of host geology units[45]. **d** A histogram of the host unit of weathering sequences after area normalization.

Unusual examples of compositional stratigraphy

Compositional stratigraphy within felsic materials. Unlike Earth which contains abundant felsic continental crust and widespread mafic oceanic crust, the martian crust is seemingly dominated by basalt and basaltic materials, including mafic-ultramafic lavas, pyroclastics, impactites, and sedimentary rocks[46]. Therefore, most weathering profiles on Mars formed in mafic-ultramafic host rocks and regolith, but if the chemical weathering process was truly global, there should be some rare examples of weathering profiles within the few felsic terranes that do exist on Mars.

Here, we show weathering profiles within felsic materials on massifs around the Hellas Basin (Fig. 3). These massifs are likely to have formed as uplifted or exhumed crust following the Hellas basin-forming event around 4.0 Ga[47]. While the massifs contain a mélange of rock types, one of the notable lithologies is the anorthosite, or a rock type rich in Fe-bearing, Ca-rich plagioclase feldspar[48]. In HiRISE images, the felsic rocks lack bedding and appear massive, similar to plutonic rocks. The broad minimum in CRISM data at ~1.25–1.3 μm is the diagnostics characteristics of Fe^{2+} in these anorthosites, ironically tracing the occurrence of the felsic materials (which is rich in Ca^{2+}, allowing substitution of Fe^{2+} for calcium). Interestingly, portions of the felsic unit show signs of alteration with a doublet absorption at 2.17 μm and 2.21 μm characteristics of Al–OH in kaolinite. Similar associations between Al clay minerals and felsic crust have been detected on Xanthe Terra and Noachis Terra. It's likely that these Al clay minerals form from felsic precursors, as previously suggested[48,49]. This setting shows that Al clay minerals occur at the top of the >2.5 km high massif, that Fe/Mg smectites occur at lower elevations, topographically higher than the lowest materials which is the plagioclase-rich felsic unit. Therefore this example appears to be a case where precipitation-driven chemical weathering of felsic protolith occurred at high elevations among martian mountains.

One single climate transition or multiple climate excursions?. Our global assessment of weathering profiles considered three hypotheses with regard to climate and compositional stratigraphy. Hypothesis #1 involves a single climate excursion and a single mineralogical transition recorded in the weathering profiles

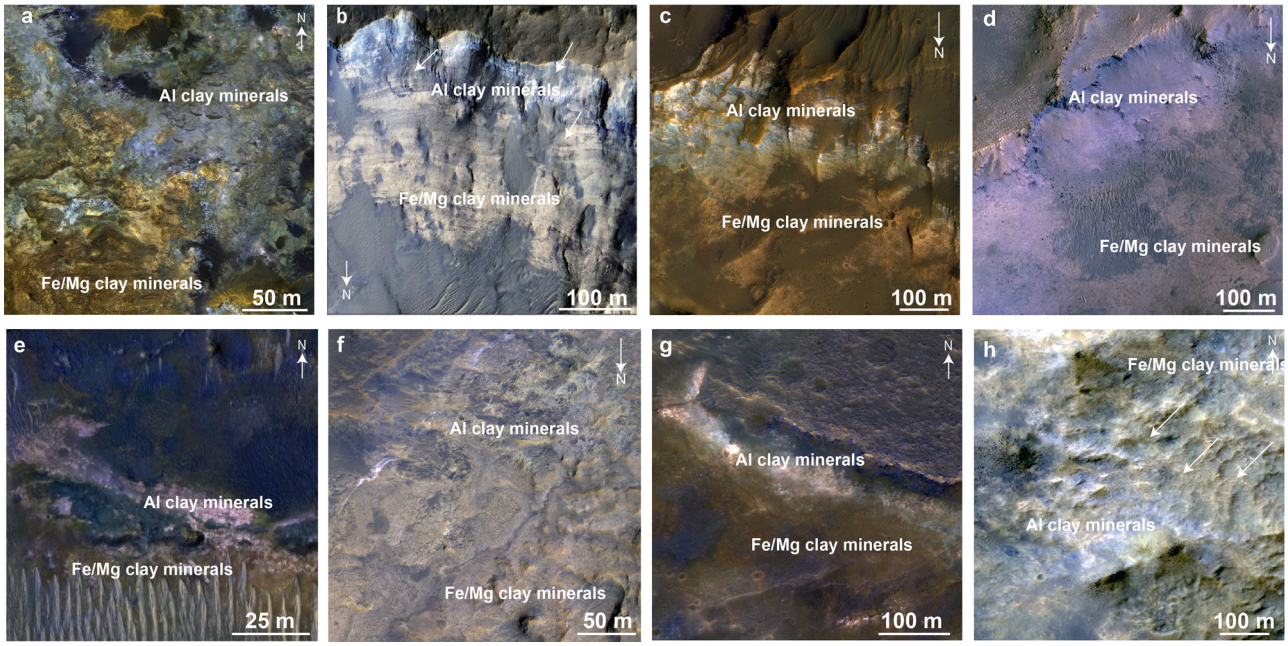

Fig. 2 Characteristics of representative geological contacts in martian weathering profiles. HiRISE IRB data (infrared, red, and blue-green) reveal submeter compositional differences of geological contacts of weathering profiles in false color. **a** Mawrth Vallis; **b** Northern Hellas Basin region; **c** Eridania northern basin; **d** Noachis Terra; **e** Nili Fossae region; **f** Terra Tyrrhen; **g** Valls Marineris; **h** Simois colles. HiRISE High-Resolution Imaging Science Experiment.

(Fig. 4a). Hypothesis #2 is that a cold, dry Noachian climate inhibiting the formation of weathering profiles was punctuated by multiple or many episodes of intense chemical weathering activity[50] (Fig. 4). In this scenario, we expected to find outcrops with multiple repetitions of Al clay and Fe/Mg clay pairs or transitions representing multiple buried events with interbedded periods of accumulation of eolian or volcanic deposits with little detectable weathering signatures (Fig. 4a). Hypothesis #3 is a hybrid of hypothesis #2 involving chemical resetting. It is likely that the porosity and permeability of the clay-bearing, possibly pyroclastic horizons is high, allowing water to move through and react with the regolith on geologically short time scales. In this scenario, multiple events and multiple profiles might form, but the uppermost Fe clay minerals could be rapidly erased during the most recent climate event as Fe was dissolved from the highest parts of the profile. In this way, Fe always moved down during weathering events, and multiple clay horizons would be reset to a single weathering profile pattern.

The results show that 201 out of 203 weathering horizons analyzed throughout the southern highlands in this work show one Al-rich layer (blue layer) overlying one Fe/Mg-rich smectites layer (red/brown layer). Only two locations show evidence of Fe/Mg smectites stratigraphically above Al-rich clay minerals on Mars, including the cases of Meridiani Planum in this study (Fig. 5) and the examples of the southern part of Coprates Chasma[39].

The case of Meridiani Planum shows a clear stratigraphic relationship between Fe/Mg/Al layers. The light-toned clay-rich outcrop is located on topographically high-standing terrain in the southern part of the region, close to the Opportunity rover's exploration zone[51]. This unit has been affected by intense erosion and impact cratering, and the remnants of the lower unit appear in the form of high-standing knobs. The light tone layer consists of two units, the upper unit and the lower unit, The upper unit is ~10 m thick, flat, and relatively dark compared to the lower unit (Fig. 5), and is spectrally similar to Fe/Mg smectite. The lower unit is relatively massive and filled with polygonal fractures (Fig. 5f). Some areas display box-work veins evidencing fluid flow, and their light tone suggests they could potentially be filled with sulfate. A sequence of Al clays overlaying Fe/Mg smectite is identified in the lower units as well. The ~80 m-thick lower unit displays a typical weathering profile with a transition from Al clays to Fe/Mg-rich smectite with a strong positive slope in 1–2 μm region, but the upper unit represents an unusual example of Fe/Mg-rich smectite overlying the Al clays. Differences in textures potentially suggest different lithologies in the host rocks, but the gradual color changes in the HiRISE data suggest a gradual compositional contact. This outcrop is one of the rare examples suggesting that at least two independent pedogenic episodes occurred.

Over 99% of the weathering profiles examined display one mineralogical transition, which might suggest that they all formed during one climate transition. But, a chemical resetting model (Fig. 4c) should not be ruled out as this scenario would produce an integrated geological record similar to the single transition model. In addition, other possibilities exist related to observational biases and limits of spatial resolution. We typically do not see 100 s or 1000 s of m of outcrop exposed, so it could be that each exposure where we can detect the weathering profiles are so poorly exposed that they do not reveal to us multiple transitions, even if they are present. With these models and questions in mind, we turn to estimates of the duration of chemical weathering events, as constrained by weathering profiles.

The time span of intensive chemical weathering. What are the oldest and youngest examples of weathering profiles, and what do these examples mean for the duration of climate conditions conducive to intense chemical weathering? Weathering profiles are usually exposed over small area, making them difficult to date directly using impact crater counting. The weathering profiles are often associated with cap units, which are better exposed over larger areas and can be dated to constrain a minimum age. Further, understanding the geologic context and relative timing within a region helps to provide age constraints.

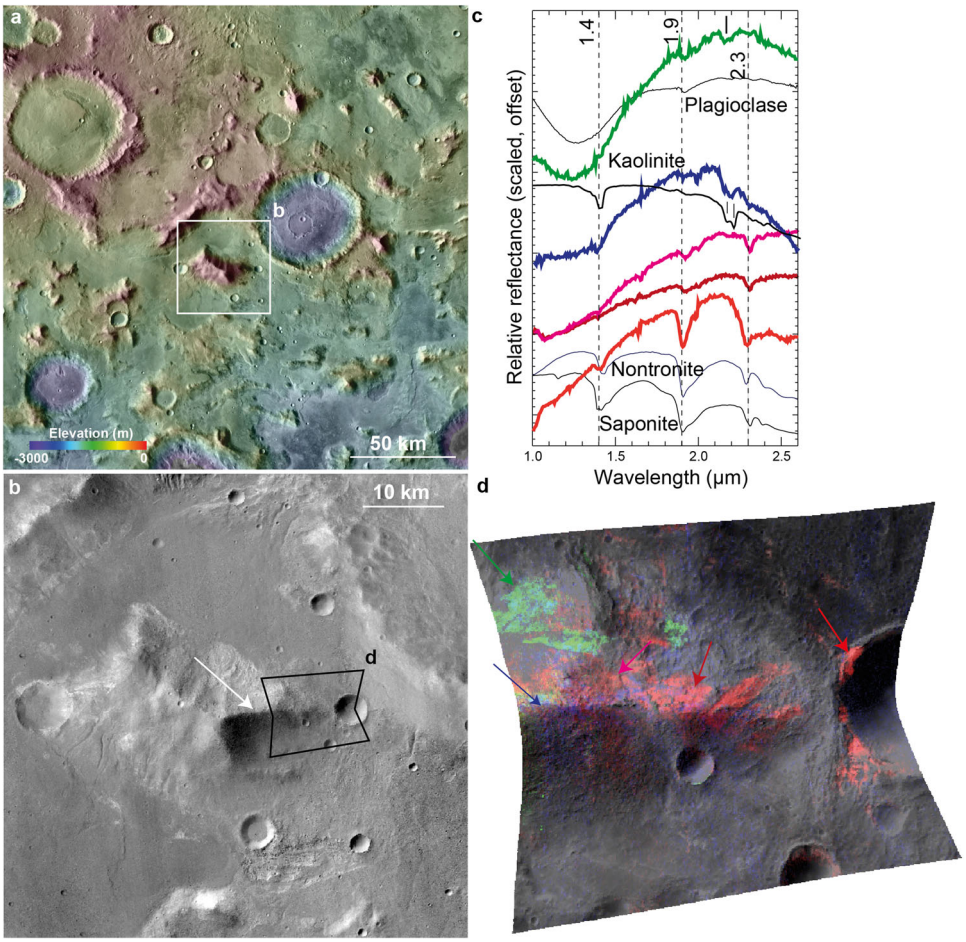

Fig. 3 Example of possible precipitation-driven chemical alteration of felsic materials. a The geology context of compositional stratigraphy on the massif of northern Hellas Planitia (66.32 2°E, 25.21°S). MOLA elevation data are draped over THEMIS daytime infrared data (warm colors are at higher elevations and cool colors are at lower elevations). **b** Close-up view of the massif indicates the location of compositional stratigraphy (white arrow). **c** Ratioed CRISM I/F spectra contain Al clay minerals, Fe/Mg smectites, and felsic materials. **d** CRISM mineral map shows the distribution of diverse altered minerals: Fe/Mg smectites in red, felsic materials in green and Al clay minerals in blue. The different color arrows show the locations of spectra acquired.

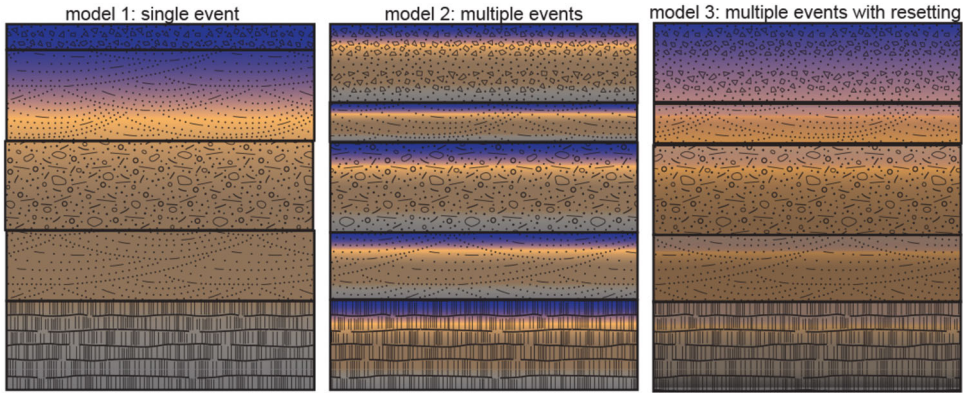

Fig. 4 Hypotheses for the pattern within weathering profiles for Al/Si materials and Fe/Mg clays. A scenario of a single climate transition (left) and another case of multiple repeated climate transitions spread out over geologic time (center panel). A third hypothesis is that multiple events occur, but the latest event chemically overwrites older weathering profiles as Fe migrates downward in the section. The blue tone unit refers to Al/Si (Fe-poor) materials, and the warm brown color indicates the occurrence of Fe/Mg smectites.

Dating the cap units associated with computational stratigraphy through the southern highlands reveals a wide range of model ages, but most are ~3.8–3.6 Ga, which is consistent with previous results[14]. The youngest example corresponds to weathering profiles found on the floor of the125 km diameter Orson Welles crater (~0.2 °S, 45.9 °W) in Xanthe Terra. This crater, which is breached by a series of fissures and graben to the southwest and by the Shalbatana outflow channel to the northeast, has a modeled age of ~3.57 Ga based on the analysis of 76 craters superimposed on the rim and ejecta materials. A

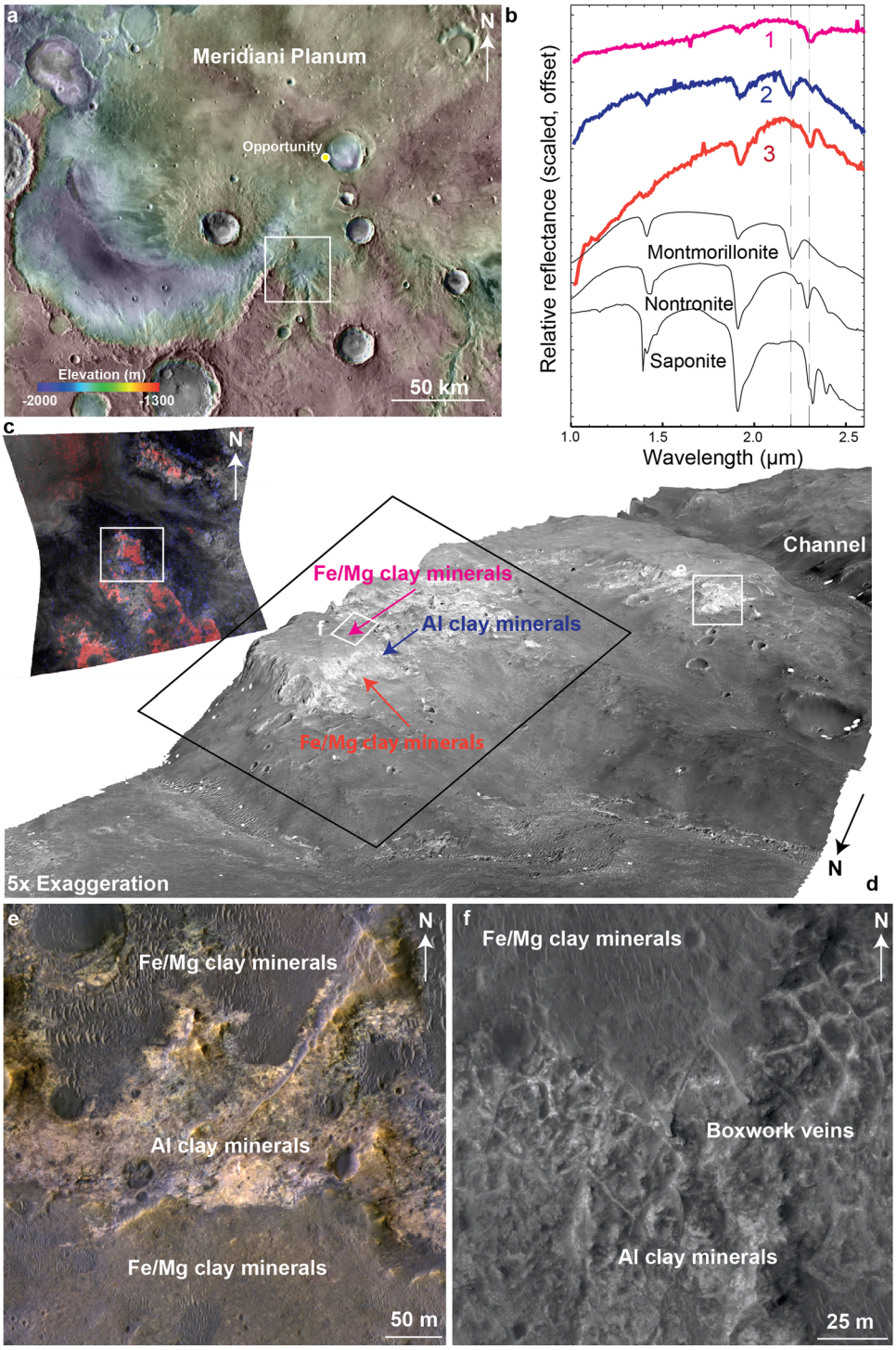

Fig. 5 Evidence of multiple pedogenic events in southern Meridiani Planum. a The geologic context of weathering profiles on an interfluve in southern Meridiani Planum. MOLA elevation data draped over THEMIS daytime infrared data (warm colors are higher elevation and cool colors are lower elevations). **b** CRISM data extracted from regions of interest are shown as offset ratio spectra compared to laboratory spectra of relevant minerals. **c** A CRISM mineral parameter map shows the distribution of Fe/Mg smectites and Al clay minerals (Fe/Mg smectites in red and Al clay minerals in blue). **d** 3D view of weathering outcrops is shown in the rectangle of **c**. with 5 times vertical exaggeration. The different color arrows show locations of spectra acquired. **e** Close-up view of HiRISE image shows the morphology and contact of clay-rich outcrops. **f** The subset of HiRISE images exhibits pervasive boxwork veins on the Al clay minerals unit.

~200 m-thick deposit of layered sedimentary crater fill materials is younger, with a model age of ~3.18 Ga (Fig. 6c). Spectra of several chaotic outcrops, exhibit a top horizon of Al/Si-rich deposits having a diagnostic absorption around 2.20 μm overlaying Fe/Mg-rich smectites with a 2.30 μm absorption feature. The upper unit has a broader asymmetric 2.20 μm absorption, suggesting the presence of opaline silica or allophane/imogolite common in weathered volcanic ash[41]. The presence and preservation of amorphous materials imply a cold and water-limited environment at that time[33,52].

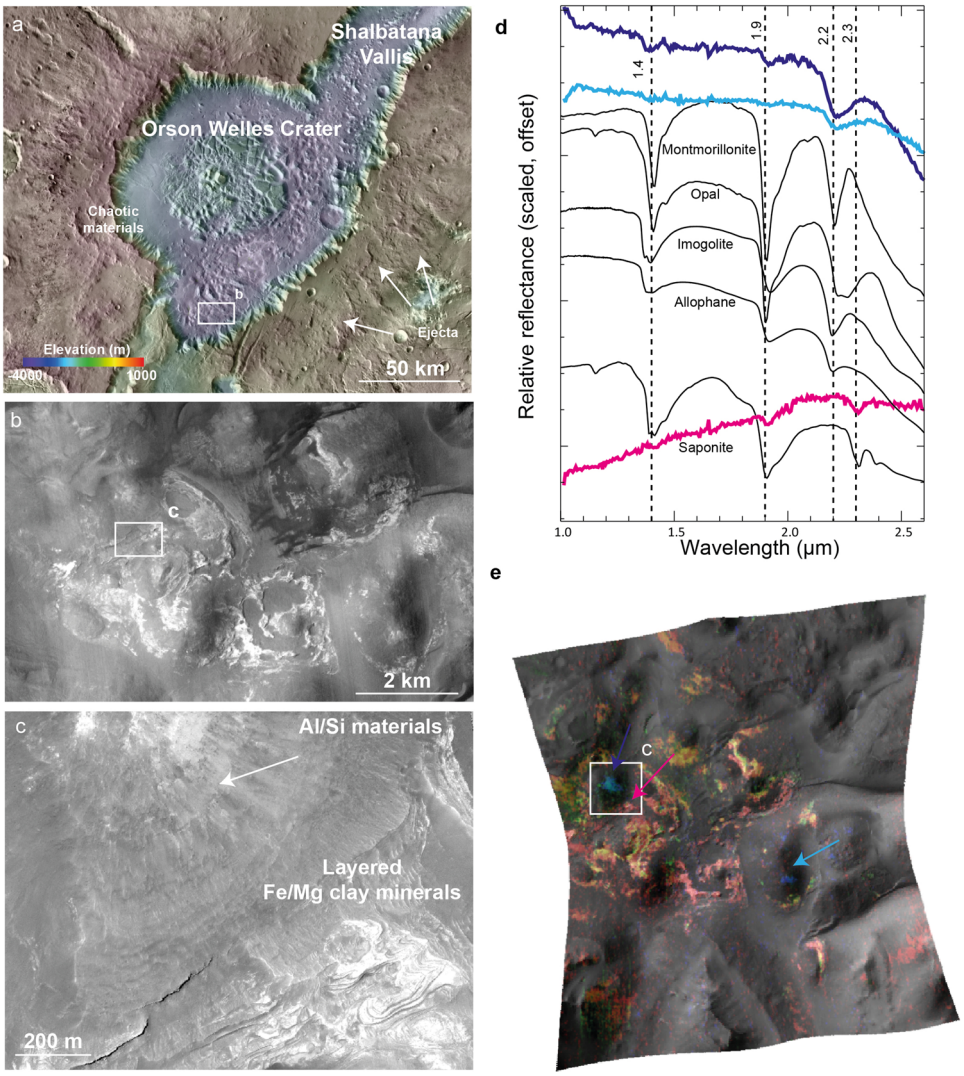

Fig. 6 The youngest known example of compositional stratigraphy on Mars. a The geology context of compositional stratigraphy on the chaotic materials in the Orson Welles crater. MOLA elevation data draped over THEMIS daytime infrared data (warm colors are higher elevations and cool colors are lower elevations). The white arrows indicate the presence of impact ejecta. **b** The CTX shows the overview of layered light-toned compositional stratigraphy. **c** Close-up HiRISE image shows the morphology and texture of compositional stratigraphy. **d** CRISM spectra extracted from regions of interest are shown as offset ratio spectra compared to laboratory spectra of relevant minerals. **e** The CRISM parameter map shows the distribution of alteration minerals, Fe/Mg phyllosilicate in red/yellow and Al phyllosilicate in blue. The different color arrows show locations of spectra acquired.

An important caveat to consider is that it might not be possible to distinguish between the age of deposits in which a weathering profile occurs and the age of the chemical weathering event itself. In other words, if the age of the layered basin fill is ~3.18 Ga (Supplementary Fig. 18), this provides an upper limit on the age of the chemical weathering occurring within those deposits. The key point is that this example represents the best evidence for a Late Hesperian chemical weathering event—the youngest known on Mars.

The oldest examples, to our knowledge, are cases of precipitation-driven weathering of pyroclastics located on ancient explosive volcanoes in Thaumasia Planum[41]. Crater counting results suggest absolute model ages for these two volcanoes in Thaumasia Planum are 3.97 Ga and 3.83 Ga, respectively (Supplementary Figs. 2 and 3). In addition, these volcanic structures also show signature of remanent crustal magnetization[53], suggesting the volcanism was pre-Noachian or early Noachian. But as descried above, it can be difficult to distinguish between the age of the volcanic deposits themselves and the age of the weathering event that altered the clastic material to clay minerals. This site nonetheless represents the oldest terrain in which a weathering profile is observed, based on crater counting results.

The examples of Thaumasia Planum and Orson Welles crater provide two essential markers for the timing of compositional stratigraphy formation (Fig. 7). Taken together, our results indicate that events marking widespread in-situ intensive chemical weathering driven by precipitation span the whole Noachian, from the Early Noachian to Late Hesperian. This striking result provides some clarity on the range of timing of climate change or excursions based on the evidence of craters counting results and cross-cutting relationships but also emphasizes some big questions surrounding the duration of chemical weathering events.

Duration of intense chemical weathering. Multiple authors have attempted to quantify the timescales of ancient aqueous activity on Mars from different perspectives, including geomorphic analyses[54–56], numerical climate modeling[57], or chemical alteration models[50]. Unifying timing constraints from theoretical and

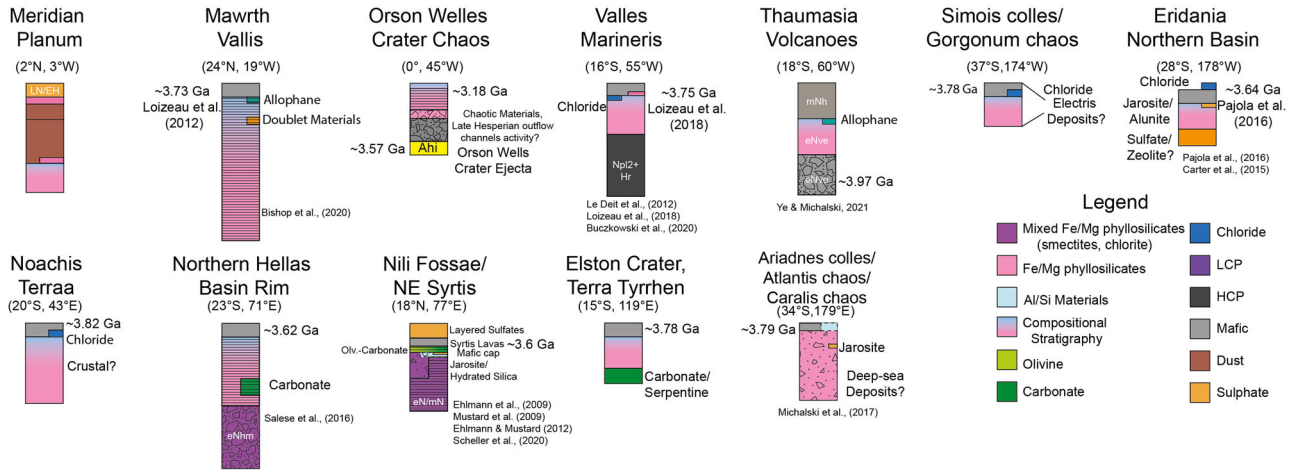

Fig. 7 Regional stratigraphy of compositional sequences on Mars. Updated regional stratigraphies from different locations on the planet – Nili Fossae/ northeastern Syrtis[22,27,40], Valles Marineris[28,29,37,39], Mawrth Vallis[18–21,23,24,32,33,38], Terra Meridiani, Northern Hellas Planitia[35], Western Terra Tyrrhen, Noachis Terra, Terra Sirenum, Orson Welles crater, Eridania northern basin[14,34], Simois colles/Gorgonum chaos, and Ariadnes colles/Atlantis chaos/ Caralis chaos[36] (latitudes and longitudes as shown). The ordering of stratigraphic columns are arranged based on longitudes. This figure is purely schematic to show the complexity of weathering processes on Mars; individual sections and units are not to scale. The blue tone unit refers to Al-rich materials and the warm brown color indicates the occurrence of Fe/Mg-rich smectites. The age of specific geologic units is shown.

geological perspectives remains a top priority of Mars researchers[1,2]. Here we integrate the results from the global assessment of weathering profiles into the big picture of the timing and duration of an ancient warmer, wetter maritan climate.

Chemical weathering resulting in thick clay-bearing pedogenic profiles represents robust and direct evidence for a climate warm enough to allow for aqueous chemical weathering. The observational biases associated with remote sensing means that we can only currently detect deposits that have 10 s of meters outcrop width (apparent thickness); smaller exposure deposits would likely escape detection with CRISM and HiRISE. Weathering profiles of 10 s of meters thick are substantial by terrestrial standards considering that pedogenic profiles on this planet are often meters-thick or less, and that long-lived chemical weathering events might be removed by subsequent physical erosion.

In many settings on Earth, average clay formation rates are commonly ~0.01 mm yr^{-1} [58], and some terrestrial clay formation rates can exceed 0.05 mm yr^{-1}. Estimating the time required to form the thickest clay deposits of Mars, a ~120 m-thick weathering profile with ~15% clays only requires <10% of the length of the Noachian period (Fig. 8)[50]. In fact, weathering profiles on Mars are rarely thicker than 100 m and generally 50–60 m thick with surficial Al-rich clay minerals[14,21,34,37]. If we consider the time span of intense weathering based on this study (from pre-Noachian/early Noachian to late Hesperian), the intense weathering period would account for an even smaller percentage. In other words, it might only have required ~10^6–10^7 years to form a weathering profile, or <1–2% of the 7×10^8 years duration in the range of time over which the weathering events occurred.

Figure 8 shows the timescales of the duration of Noachian time and the range of ages of chemical weathering profiles. For comparison, the time required for the formation of some classic weathering localities on Earth are shown[26,59,60]. Also shown are constraints from modeling of mineral dissolution rates[61–63], clay formation rates[50,58], and geomorphological activity (delta and alluvial fan formation[55,64–67], erosion of valley networks[54], and duration of channel-fed basins[56,68]). The timing of these events are all compared to the duration of climate warming episodes based on theoretical models[3,6,7,69,70].

The thickness of weathering profiles and estimates of clay mineral abundance provide only a very coarse constraint on the duration of weathering events with many caveats. First, weathering reactions cannot propagate indefinitely owing to a decrease in the diffusion rate of dissolved cations with reaction progress[71]. Second, weathered rocks are often more easily disaggregated by physical erosion. Third, chemical weathering rates present a rough tradeoff between duration and temperature, but with many complexities[50]. Though it is an oversimplification, it is likely that short-term climate excursions to higher temperatures with high water/rock ratios would produce dramatically thicker deposits than long-duration events at a low temperature barely above freezing[50].

Further, a major factor that is difficult to tightly constrain pertains to lithology, permeability, porosity, and overall susceptibility of weathering of the host rock in which the weathering profile occurs. It is important to note that explosive volcanism and impact events likely dominated early episodes of the geologic history of Mars and weathered materials might be widely composed of ash or impact glass[72–74]. The amorphous, fragmented, mafic, porous, reactive ash/impactites composed of particles with high specific surface area would have been much more susceptible to alteration in shorter times than nearly any other rock type, which could accelerate the weathering process substantially, up to several orders of magnitude[41,61,75–77].

Some sections also exhibit clear sedimentary features, such as cross-bedding, layered, inverted channels, and craters (Fig. 9), indicating a complex history with periods of transportation, burial, cementation, exhumation, and erosion. Pedogenic leaching could have altered the mafic/ultramafic protolith in some places both before and after physical transport[39].

Conclusions. This global survey evaluates the mineralogy, geologic context, and age constraints of >200 examples of compositional stratigraphy on Mars to constrain the timing of intense chemical weathering associated with past climate. The youngest might be Early Hesperian, but most of them are >3.7 Ga. The fact that weathering profiles occur at a wide range (>11 km) of elevations, from −5 to 6 km, suggests they formed as a function of top-down, precipitation-driven chemical weathering and the fact that they occur throughout the ancient crust indicates that the phenomenon was global in scope.

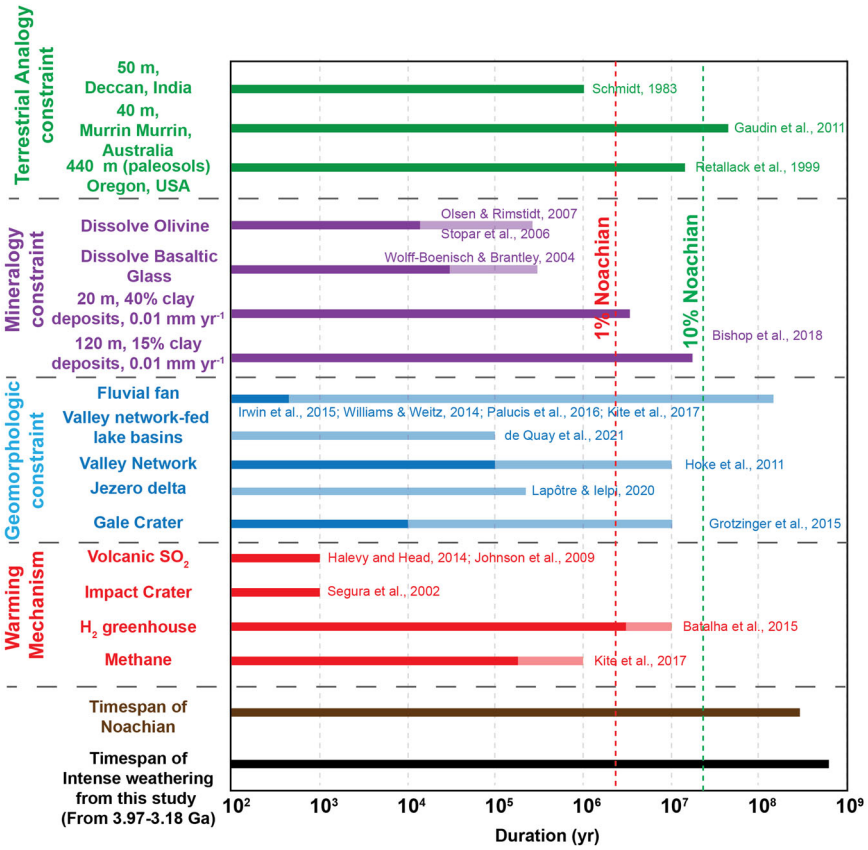

Fig. 8 The timescales of warming mechanisms, geomorphologic constraints, mineralogic constraints, and constraints from terrestrial analogs from the previous studies[3,7,26,50,54,56,59–61,68,69,102]**.** A dark color bar indicates the minimum duration of warming event, geomorphologic constraints and mineralogy constraints, while the light color bar suggests the maximum duration of these constraints. This timeline of Mars process utilizes the Neukum chronology models[93]. Period boundary (green line) is as defined by Werner and Tanaka[91].

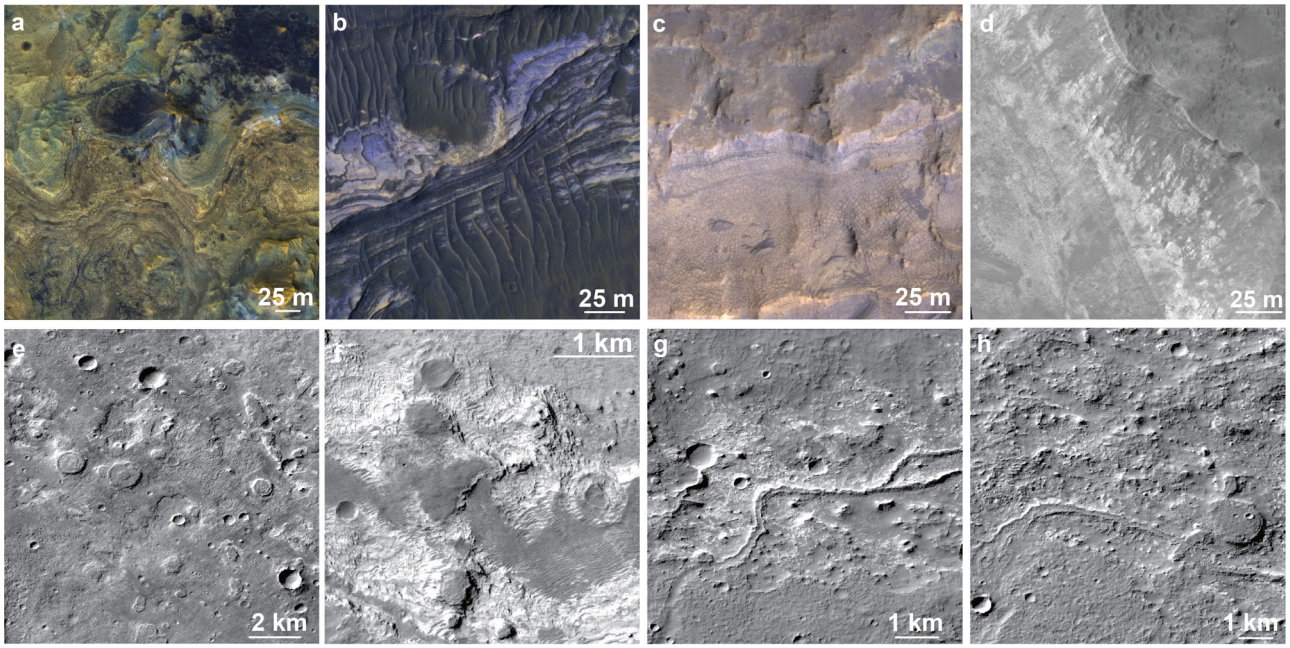

Fig. 9 Evidence of sedimentary process on or within weathering profiles on Mars. Layer structures of weathering profiles (**a**–**d**). Inverted craters (**e**, **f**) and inverted channels on weathering outcrops (**g**, **h**).

Most of the weathering profiles display only one observable mineralogical transition, which in itself is most consistent with a single climate transition event. However, geochemical resetting is a legitimate possibility, as described above. The diverse mineral assemblages within the weathering sequences demonstrate that the aqueous settings were perhaps complicated, varying in some ways from site to site or through time. In some cases, Al-rich deposits are also associated with hydrated silica, jarosite, and alunite, which indicate an acidic, oxidized formation environment[34,38,78] and likely implies an acid weathering scenario[79]. Further, the presence of allophane/imogolite implies neutral to weakly acidic, water-limited environments (pH 5–7)[33,80]. According to Bultel et al.[81], evidence of carbonate was found in weathering sequences, suggesting a neutral aqueous environment and arid climate.

Warm climate excursions lasting 10^6–10^7 years driven by reduced greenhouse gases are the most viable solution and consistent with the current observed weathering sequences on Mars. The geochemical consequences of an anoxic reducing atmospheric environment would predict separation of Fe from Al from top to bottom in weathered rock because Fe is mobile while Al is immobile under such conditions[18]. Fe is the most important factor governing color in HiRISE images, and such a top-down process related to Fe mobility is can explain the false color patterns. The diffuse color patterns crosscutting the physical stratigraphic bedding strongly suggest these weathered rocks formed under an anoxic reducing atmospheric environment.

Estimates of the duration of time required to form a typical weathering profile (~millions of years) amount to only a small fraction of the Noachian period. Therefore, the wide range of estimated ages spanning ~700–800 My appears inconsistent with a single climate transition event. It might be that multiple climate excursions occurred but enhanced Fe-mobility from the HiRISE color imagery data under a reduced atmosphere at that time allowed for subsequent climate excursions to chemically overwrite older weathering horizons resulting in an integrated geologic record misleadingly showing evidence for just one event, the latest event affecting that area.

Weathering profiles may have been linked to other geomorphological features at that time, such as degraded impact craters, valley networks, closed-basin lakes, and open-basin lakes. An example is presented of a weathering profile (101.52 °E, 0.2 °S) draped on the high-standing interfluves of valley networks. But, Howard and Moore[82] and Wray et al.[21] conclude that Mawrth Vallis cross-cut the weathering sequences, indicating the weathering event predates the latest fluvial activity in that area. The exact timing of these processes is hard to assess in geologic records because valley networks are destructional erosional features, which would destroy the building-up of weathering profiles. The most plausible scenario is that major weathering events are roughly contemporary with a pulse of enhanced valley networks formation (Fig. 10) in the Late Noachian/Early Hesperian[42,83–85].

While most channels or lakes might have been active for only 10^3–10^6 years[86], the weathering horizons perhaps required 10^6–10^7 years to form, providing a slightly stronger constraint on the duration of aqueous activity. An interesting and important contradiction in the geologic record of Mars is that the range of time of near-surface weathering is surprisingly long but the timing required to form each weathering profile was likely relatively short. This conundrum might reflect poor exposure or preservation of the geologic record. We argue that the occurrence of weathering profiles in many geologic units at a wide range of ages over a large period of geologic time and at a wide range of elevations, indicate a global climatic process involving top-down, precipitation-driven chemical weathering. An important element of this process was likely Fe-mobility, which can be geologically rapid under reducing conditions. These results, therefore, point to weathering driven by reduced greenhouse gases on ancient Mars where multiple events resulted in the Fe-loss from the uppermost geologic record.

Methods

Visible Imagery data. Context Camera (CTX) and corrected mosaics[87] was used to provide general geological context for compositional stratigraphy at 6 m/pixel. Detail geomorphologic characteristics of compositional stratigraphy are analyzed using High-Resolution Imaging Science Experiment (HiRISE) images with a spatial resolution of 0.25 m/pixel. HiRISE is equipped with a red filter for panchromatic images and NIR and blue-green filters for color images[88]. The central wavelength of the red filter is 694 nm, the blue-green filter is 536 nm and the NIR wavelength is 874 nm. The color images of HiRISE are powerful to identify compositional and roughness variations at sub-meter scales. Additional THEMIS daytime and nighttime infrared mosaics images with 100 m/pixel provide contextual and qualitative thermophysical properties of the surface materials[89].

Hyperspectral imagery data. The mineralogy of compositional stratigraphy was investigated using visible/near-infrared reflectance data from the Compact Reconnaissance Imaging Spectrometer for Mars (CRISM). CRISM is a hyperspectral imaging spectrometer with visible and near-infrared (VNIR) detectors spanning ~0.4–3.9 μm, covering approximately 10 km × 10 km with a spatial resolution of 18 m/pixel in full-resolution targeted mode[90]. Raw CRISM I/F data is downloaded from Planetary Data System (PDS) and then processed through the CRISM Analysis Toolkit v7.4 for viewing geometry calibration and atmospheric correction following the standard procedures[27]. Spectral parameters are calculated for each processed data to spatially map the strength of diagnostic absorption features of minerals and mineral classes related to Al-OH, Fe/Mg-OH, and H_2O[91]. I/F spectra extracted from individual or groups of pixels were ratioed against data of spectrally unremarkable terrain in the same image, as a means to extract spectral shapes and validate mineral parameter maps.

Topography data. The regional topography was investigated using a blended MOLA/HRSC gridded topographic map with a resolution of 200 m per pixel. We also used Ames Stereo Pipeline (ASP)[92] to generate high-resolution CTX and HIRISE DEMs, in order to constrain the stratigraphy relationship and thickness of compositional stratigraphy when possible.

Weathering sequence catalog. In this worst, firstly, we complied the potential weathering profiles from previous studies[14,15,19–41] and search for additional weathering sequences based on hydrous mineral database of Carter et al.[17] to get more comprehensive understanding of global distribution of compositional stratigraphy. Then, we used corrected CRISM data and spectral parameter map to confirm the occurrence of Fe/Mg smectites and Al clays and representative spectra is extracted. The Fe/Mg phyllosilicates is the most common hydrous minerals on Mars. Spectra parameters D2300, which is used to characterize the diagnostics features of Fe/Mg smectites around 2.30 μm. This spectra index can delineate the distribution of Fe/Mg smectites. Due to the small exposure of Al clay minerals, the BD2200, which can capture the signature of Al clay minerals, allophane, imogolite, and hydrated silica around 2.20 μm, is usually noisy and therefore they are generally overlooked in previous. We used HiRISE color image to analysis the color difference within clay-rich deposits that may indicate possible compositional heterogeneity. Then, spectra were extracted from CRISM data of this region of interest to confirm the presence of Al/Si materials, such as montmorillonite, kaolinite, hydrated silica, and amorphous materials. CTX, HiRISE, MOLA/HRSC DEM, HiRISE DEM (if available), CTX DEM (if available) and CRISM data were incorporated into a Geographic Information System (GIS) environment and were co-registered to study the geology and mineralogy characteristics.

Crater-counting and constraints on surface ages. Counts of superposed craters and models of crater production for Mars were used to evaluate relative ages and absolute model ages of specific geology units[90,91,93]. Crater counts were performed on publicly available CTX mosaic images produced by The Murray Lab of Caltech.

The CraterTools extension for ArcMap was used to map superposed craters. For each crater, a best-fit circle was mapped, and the crate's diameter was determined in a local sinusoidal projection, providing an accurate measurement of crater's diameter[94]. Craters with a raised rim and depressed center are included for model age determination. Secondary craters, such as highly clustered craters or craters occurring in chains, were omitted from age determination. Small craters were not included in the final analysis because they are strongly affected by the obliteration process[93]. According to Warner et al.[95], the crater-counting area should exceed 1000 km^2, and all counting areas are larger than 1000 km^2 in this study, and the average counting area is 8089 km^2. In this paper, only craters larger than 1 km in diameter were used in the model age determinations for the majority of geology units. But, a portion of regions have very few craters larger than 1 km, so

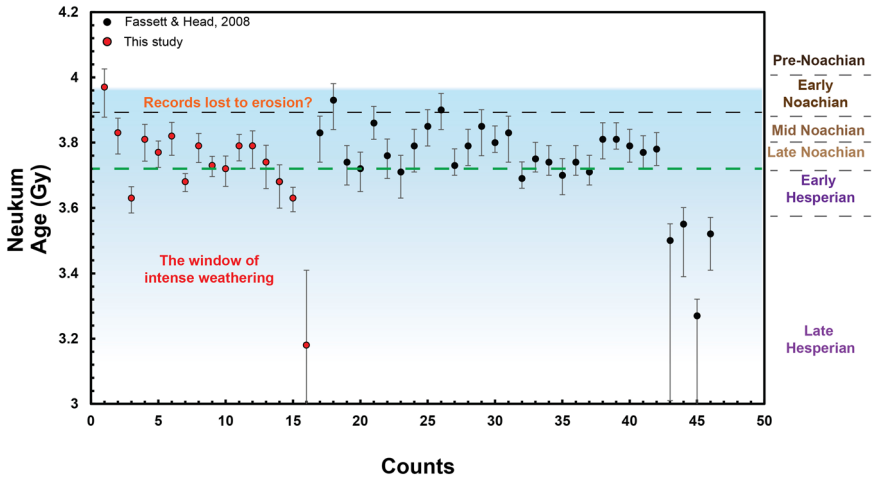

Fig. 10 A summary of the age constraint of weathering sequences compared to the age of valley network formation. The red dot represents the crater-counting age constraint of weathering sequences (Supplementary Table 2 and Supplementary Figs. 2–18). The black dot indicates the ages for the cessation of valley networks. Model age errors are +/−1-sigma error on the model fit for N(1). Period boundary (green line) is as defined by Werner and Tanaka[91]. Prior to ~3.9 Ga, the planet was likely too geologically active to retian much of the geologic record of chemical weathering or sedimentary processes.

a smaller diameter range was used to ensure that at least 5 counted craters were used in the model age determination. The smallest crater diameter included in our modal age calculations was 800 m. Model age determination was made using the production function of Ivanov[90] and the chronology function of Hartmann and Neukum[93]. Period determination was calculated from the stratigraphic age boundaries according to Werner and Tanaka[91].

We note that crater counting of small areas comes with uncertainties[96,97]. Specifically, counting of small craters (e.g., <4 km) in ancient terrains can result in ambiguous age constraints[98]. We have made efforts to maximize the counting area while also remaining conservative to be sure the counting area represents the geologic units in question. Similarly, we made an effort to use the largest craters possible for age constraints. Despite these efforts, there are unavoidable uncertainties in the crater age dating approach used here, but we point out that this method is only one of the techniques used to constrain geologic age in this study. In many cases, stratigraphic relations and superposition may provide reliable age constraints.

Constraints of terrestrial analogs, mineralogy, geomorphology and warming mechanisms. The John Day Formation in eastern Oregon contains volcaniclastic paleosols, which forms during Eocene-Oligocene (43–28 Ma)[60]. The ~400-m-thick stratigraphic column contains over 500 individual clay mineral-rich (30–95 wt.%) paleosols spanning 15 Myr through the climatic change of the Eocene–Oligocene boundary[13]. The mineralogy of paleosols from the Eocene/Oligocene-age Clarno and John Day Formations preserves a record of dramatic climate change. The mineralogy changes from high kaolinite and oxide abundances at the bottom (warm and wet Eocene) to high smectite abundances (drying late Eocene) in the middle to poorly crystalline phases at the stratigraphic top of the section (cool and dry Oligocene). The Deccan Volcanic Province is one of the world's largest continental flood basalt provinces and its eruptions straddle the Cretaceous-Tertiary boundary (64–67 Ma)[99]. As the India plate traveled past the equator, these basalts were extensively altered and leached, resulting in deep weathering profiles and laterites. The laterites (with an overall thickness of 50 m) developed between 10–20 My after the lavas were emplaced and formation probably stopped when India collided with Asia and the region was uplifted, according to paleomagnetic evidence[59]. The Murrin Murrin profile is located in southern Australia and developed in Archaean (2.7 Ga) serpentinized peridotite massifs. The weathering profile has an overall thickness of 30–40 m. It is composed of three main zones identified from bottom to top: saprolite, smectite, and Al-rich zones. The formation of Murrin Murrin weathering profiles is considered to have formed in the late Cretaceous to early Tertiary[100].

According to Olsen and Rimstidt[63], if we consider 1 mm (radius) forsterite grain in an such an environment (T = 25 °C) at pH 7.5. The olivine particle would last 3 Myrs including a 100 x lab-to-field correction would be appropriate. If we consider a 1 mm forsterite grain at 25 °C and pH 3.5, its reference lifetime would be approximately 14,000 years. Warming the surface of Mars requires a relative thick atmosphere, at least 1 bar CO_2 mixed with few percentages of hydrogen. Thicker atmosphere, which is needed for most ways to warm the planet, implies a lower pH and thus shorter lifetime for olivine. Higher temperature would also speed up the dissolution process. The experiment shows that the lifetime of olivine grain increases by about ten times from 0 °C to 25 °C. If olivine was more iron-rich, as seen in various Martian meteorites[101], maximum residence times would be further reduced. The estimation of the minimum residence time offers lower boundary conditions[62]. The residence time of a 1 mm forsterite at 25 °C is ~420,000 years at pH 7, including 100× lab-to-filed correction. Some calculations give olivine lifetimes in fluids at Mars' surface as short as 10 years if we consider the most favorable conditions, including low pH, high temperature and small grain size. The early Mars likely dominate by explosive volcanism and experienced heavy impact process, and therefore glass would be the import constituent of Martian crust[41,72]. The lifetime at pH 4 and 25 °C of a 1 mm basaltic glass sphere is 50,000 years, while the more Si-rich rhyolitic glass is 450,000 years when considering the lab-to-field correction[61]. Because the silicate content of glass affects the glass dissolution rate substantially, we consider the basaltic glass could serve as the minimum residence time and more Si-rich composition is used as the maximum time. In order to provide a general sense of clay deposition equivalent to 1% and 10% Noachian period, the duration of tens to hundreds of meters clay deposits are calculated using the common clay formation rate on Earth. Average clay formation rates on Earth are generally ~0.01 mm yr^{-1} in many settings and can reach as high as 0.05 mm yr^{-1} in some regions, such as weathered ash deposits[50,58].

Large fluvial fans are compelling evidence for surface flows. Based on sediment transport rate and fan volume measurement, Eberswalde delta took at least 15000 years to form in a lake[65]. For SW Melas Fan, the minimum lake lifetime ranges from 4000 years to 10000 years[64]. Dulce Vallis, Farah Vallis, and Gale Pancake within Gale crater the lake has been there for at least 500 years, 6000 years and 3000 years, respectively[66]. Kite et al.[67] used embedded craters within fluvial fan provides a lower boundary for alluvial fans formation timespan, requiring >100–300 Myr. But, these fans might active intermittently, and the actual aqueous activity might only contain a small portion of this time span. Using the three different sediment transport models, Hoke et al.[54] found that the formation timescales of martian valley networks range from 10^5 to 10^7 years. According to ref. [56], combining hydrological balances with precipitation outputs from climate models, the breaching runoff episode likely lasted 10^2–10^5 years. Jezero impact crater lake is the landing site of NASA's Perseverance rover and samples are prepared for retrieving, which will determine the absolute and exposure age of some stratigraphy units or aqueous activities to elucidate the nature regrading hydrologic and climate of early Mars. Using the stratigraphy of the Jezero delta with a new empirical relationship between the lateral migration rate of single-thread rivers and channel width, it suggests the delta formation spanned ~17–37 years over a total duration of ~380,000 years, depending on the frequency of flow activity[55]. Gale crater is the landing site of Mars Science Laboratory mission's rover, Curiosity. The investigation suggests individual lakes of Gale crater were stable on the ancient surface of Mars for sediment accumulation over 10,000 to 10,000,000 years[68].

Several warming mechanisms have been proposed: (1) Stimulating climatic effect of punctuated volcanism shows that the rapid emitting of sulphur volatiles warmed the surface for hundreds of year through the combined greenhouse effect of SO_2 and the subdued scattering effect of H_2SO_4 coatings on dust and ash grains[3]; (2) Large impact crater produced global blankets of very hot ejecta, ranging in thickness from meters to hundreds of meters, which warmed the surface, keeping it above the freezing point of water for periods ranging from decades to millennia. The duration of such warming mechanism depends on impactor size[69]; (3) Another idea suggests that early Mars could have undergone repeated long period cycles (~100 Myr each) of global glaciation interrupted by deglaciation and short intervals of transient (~5–10 Myr each) warming as early Mars cycled into and outside the outer edge limit of the habitable zone[102]; (4) Chaotic obliquity transitions might destabilize methane trapped in the subsurface, which produce episodic methane bursts, leading to lake-forming climate last 10^5 to 10^6 years[7].

Data availability

Data required to complete this work include (1) hyperspectral imagery data from CRISM; (2) visible image from Context Camera (2) high-resolution visible images from High-Resolution Imaging Science Experiment; (3) day and night-time infrared image data from THEMIS; (4) and topographic data from MOLA. All data used in this work, as well as the software used to process CRISM data, are publicly available from Planetary Data System (https://pds.nasa.com). The corrected CTX mosaic is available through the Bruce Murray Laboratory for Planetary Visualization (http://murraylab.caltech.edu/CTX/). The software for CTX and HiRISE digital elevation production is Ames Stereo 637 Pipeline (ASP) (https://ti.arc.nasa.gov/tech/asr/groups/intelligent-robotics/ngt/stereo/).

Received: 13 December 2021; Accepted: 21 October 2022;
Published online: 04 November 2022

References

1. Wordsworth, R. D. The climate of early Mars. *Annu. Rev. Earth Planetary Sci.* **44**, 381–408 (2016).
2. Kite, E. S. Geologic constraints on early Mars climate. *Space Sci. Rev.* **215**, https://doi.org/10.1007/s11214-018-0575-5 (2019).
3. Halevy, I. & Head, J. W. Episodic warming of early Mars by punctuated volcanism. *Nat. Geosci.* **7**, 865–868 (2014).
4. Ramirez, R. M. et al. Warming early Mars with CO_2 and H-2. *Nat. Geosci.* **7**, 59–63 (2014).
5. Ramirez, R. M. & Craddock, R. A. The geological and climatological case for a warmer and wetter early Mars. *Nat. Geosci.* **11**, 230–237 (2018).
6. Batalha, N., Domagal-Goldman, S. D., Ramirez, R. & Kasting, J. F. Testing the early Mars H-2-CO2 greenhouse hypothesis with a 1-D photochemical model. *Icarus* **258**, 337–349 (2015).
7. Kite, E. S. et al. Methane bursts as a trigger for intermittent lake-forming climates on post-Noachian Mars. *Nat. Geosci.* **10**, 737-+ (2017).
8. Wordsworth, R. et al. Transient reducing greenhouse warming on early Mars. *Geophys. Res. Lett.* **44**, 665–671 (2017).
9. Wordsworth, R. et al. A coupled model of episodic warming, oxidation and geochemical transitions on early Mars. *Nat. Geosci.* **14**, 127-+ (2021).
10. Craddock, R. A. & Howard, A. D. The case for rainfall on a warm, wet early Mars. *J. Geophys. Res. Planets* **107**, 21-21–21-36 (2002).
11. Bibring, J.-P. et al. Global mineralogical and aqueous Mars history derived from OMEGA/Mars express data. *Science* **312**, 400–404 (2006).
12. Rye, R. & Holland, H. D. Paleosols and the evolution of atmospheric oxygen: a critical review. *Am. J. Sci.* **298**, 621–672 (1998).
13. Broz, A. P. et al. Mineralogy and diagenesis of Mars-analog paleosols from eastern Oregon, USA. *Icarus* **380**, 114965 (2022).
14. Carter, J., Loizeau, D., Mangold, N., Poulet, F. & Bibring, J. P. Widespread surface weathering on early Mars: a case for a warmer and wetter climate. *Icarus* **248**, 373–382 (2015).
15. Noe Dobrea, E. Z. et al. Mineralogy and stratigraphy of phyllosilicate-bearing and dark mantling units in the greater Mawrth Vallis/west Arabia Terra area: constraints on geological origin. *J. Geophys. Res.* **115**, https://doi.org/10.1029/2009je003351 (2010).
16. Ehlmann, B. L. et al. Subsurface water and clay mineral formation during the early history of Mars. *Nature* **479**, 53–60 (2011).
17. Carter, J., Poulet, F., Bibring, J. P., Mangold, N. & Murchie, S. Hydrous minerals on Mars as seen by the CRISM and OMEGA imaging spectrometers: Updated global view. *J. Geophys. Res. Planets* **118**, 831–858 (2013).
18. Liu, J. et al. Anoxic chemical weathering under a reducing greenhouse on early Mars. *Nat. Astronomy* **5**, 503–509 (2021).
19. Loizeau, D. et al. Phyllosilicates in the Mawrth Vallis region of Mars. *J. Geophys. Res. Planets* **112**, https://doi.org/10.1029/2006je002877 (2007).
20. Bishop, J. L. et al. Phyllosilicate diversity and past aqueous activity revealed at Mawrth Vallis, Mars. *Science* **321**, 830–833 (2008).
21. Wray, J. J., Ehlmann, B. L., Squyres, S. W., Mustard, J. F. & Kirk, R. L. Compositional stratigraphy of clay-bearing layered deposits at Mawrth Vallis, Mars. *Geophys. Res. Lett.* **35**, n/a–n/a (2008).
22. Ehlmann, B. L. et al. Identification of hydrated silicate minerals on Mars using MRO-CRISM: geologic context near Nili Fossae and implications for aqueous alteration. *J. Geophys. Res. Planets* **114**, https://doi.org/10.1029/2009je003339 (2009).
23. McKeown, N. K. et al. Characterization of phyllosilicates observed in the central Mawrth Vallis region, Mars, their potential formational processes, and implications for past climate. *J. Geophys. Res. Planets* **114**, https://doi.org/10.1029/2008je003301 (2009).
24. Loizeau, D. et al. Stratigraphy in the Mawrth Vallis region through OMEGA, HRSC color imagery and DTM. *Icarus* **205**, 396–418 (2010).
25. Michalski, J. R. et al. The Mawrth Vallis region of Mars: a potential landing site for the Mars Science Laboratory (MSL) mission. *Astrobiology* **10**, 687–703 (2010).
26. Gaudin, A., Dehouck, E. & Mangold, N. Evidence for weathering on early Mars from a comparison with terrestrial weathering profiles. *Icarus* **216**, 257–268 (2011).
27. Ehlmann, B. L. & Mustard, J. F. An in-situ record of major environmental transitions on early Mars at Northeast Syrtis Major. *Geophys. Res. Lett.* **39**, n/a–n/a (2012).
28. Le Deit, L. et al. Extensive surface pedogenic alteration of the Martian Noachian crust suggested by plateau phyllosilicates around Valles Marineris. *J. Geophys. Res. Planets* **117**, E00J05 (2012).
29. Loizeau, D. et al. Characterization of hydrated silicate-bearing outcrops in Tyrrhena Terra, Mars: implications to the alteration history of Mars. *Icarus* **219**, 476–497 (2012).
30. Bishop, J. L. et al. What the ancient phyllosilicates at Mawrth Vallis can tell us about possible habitability on early Mars. *Planet Space Sci.* **86**, 130–149 (2013).
31. Michalski, J. R., Niles, P. B., Cuadros, J. & Baldridge, A. M. Multiple working hypotheses for the formation of compositional stratigraphy on Mars: insights from the Mawrth Vallis region. *Icarus* **226**, 816–840 (2013).
32. Loizeau, D. et al. History of the clay-rich unit at Mawrth Vallis, Mars: high-resolution mapping of a candidate landing site. *J. Geophys. Res. Planets* **120**, 1820–1846 (2015).
33. Bishop, J. L. & Rampe, E. B. Evidence for a changing Martian climate from the mineralogy at Mawrth Vallis. *Earth Planetary Sci. Lett.* **448**, 42–48 (2016).
34. Pajola, M. et al. Eridania Basin: an ancient paleolake floor as the next landing site for the Mars 2020 rover. *Icarus* **275**, 163–182 (2016).
35. Salese, F. et al. A sedimentary origin for intercrater plains north of the Hellas basin: implications for climate conditions and erosion rates on early Mars. *J. Geophys. Res. Planets* **121**, 2239–2267 (2016).
36. Michalski, J. R., Dobrea, E. Z. N., Niles, P. B. & Cuadros, J. Ancient hydrothermal seafloor deposits in Eridania basin on Mars. *Nat. Commun.* **8**, 10 (2017).
37. Loizeau, D. et al. Quantifying widespread aqueous surface weathering on Mars: the plateaus south of Coprates Chasma. *Icarus* **302**, 451–469 (2018).
38. Bishop, J. L. et al. Multiple mineral horizons in layered outcrops at Mawrth Vallis, Mars, signify changing geochemical environments on early Mars. *Icarus* **341**, 12 (2020).
39. Buczkowski, D. L. et al. Anomalous phyllosilicate-bearing outcrops south of coprates chasma: a study of possible emplacement mechanisms. *J. Geophys. Res. Planets* **125**, e2019JE006043 (2020).
40. Scheller, E. L. & Ehlmann, B. L. Composition, stratigraphy, and geological history of the Noachian Basement surrounding the Isidis impact basin. *J. Geophys. Res. Planets* **125**, e2019JE006190 (2020).
41. Ye, B. & Michalski, J. R. Precipitation-driven pedogenic weathering of volcaniclastics on early Mars. *Geophys. Res. Lett.* **48**, e2020GL091551 (2021).
42. Fassett, C. I. & Head, J. W. Valley network-fed, open-basin lakes on Mars: distribution and implications for Noachian surface and subsurface hydrology. *Icarus* **198**, 37–56 (2008).
43. Hynek, B. M., Beach, M. & Hoke, M. R. T. Updated global map of Martian valley networks and implications for climate and hydrologic processes. *J. Geophys. Res.* **115**, https://doi.org/10.1029/2009je003548 (2010).
44. Fassett, C. I. & Head, J. W. The timing of martian valley network activity: constraints from buffered crater counting. *Icarus* **195**, 61–89 (2008).
45. Tanaka, K. L., Robbins, S. J., Fortezzo, C. M., Skinner, J. A. & Hare, T. M. The digital global geologic map of Mars: chronostratigraphic ages, topographic and crater morphologic characteristics, and updated resurfacing history. *Planet Space Sci.* **95**, 11–24 (2014).
46. McLennan, S. M., Grotzinger, J. P., Hurowitz, J. A. & Tosca, N. J. The sedimentary cycle on early Mars. *Annu. Rev. Earth Planetary Sci.* **47**, 91–118 (2019).
47. Leonard, G. J. & Tanaka, K. L. *Geologic Map of the Hellas Region of Mars* (US Department of the Interior, US Geological Survey, 2001).
48. Carter, J. & Poulet, F. Ancient plutonic processes on Mars inferred from the detection of possible anorthositic terrains. *Nat. Geosci.* **6**, 1008–1012 (2013).
49. Wray, J. J. et al. Prolonged magmatic activity on Mars inferred from the detection of felsic rocks. *Nat. Geosci.* **6**, 1013–1017 (2013).
50. Bishop, J. L. et al. Surface clay formation during short-term warmer and wetter conditions on a largely cold ancient Mars. *Nat. Astronomy* **2**, 206–213 (2018).
51. Arvidson, R. E. Aqueous history of Mars as inferred from landed mission measurements of rocks, soils, and water ice. *J. Geophys. Res. Planets* **121**, 1602–1626 (2016).
52. Du, P. et al. Effects of environmental Fe concentrations on formation and evolution of allophane in Al-Si-Fe systems: implications for both Earth and Mars. *J. Geophys. Res. Planets* **125**, e2020JE006590 (2020).
53. Lillis, R. J. et al. An improved crustal magnetic field map of Mars from electron reflectometry: highland volcano magmatic history and the end of the martian dynamo. *Icarus* **194**, 575–596 (2008).
54. Hoke, M. R. T., Hynek, B. M. & Tucker, G. E. Formation timescales of large Martian valley networks. *Earth Planetary Sci. Lett.* **312**, 1–12 (2011).
55. Lapôtre, M. G. & Ielpi, A. The pace of fluvial meanders on Mars and implications for the western delta deposits of Jezero crater. *AGU Adv.* **1**, e2019AV000141 (2020).

56. de Quay, G. S., Goudge, T. A., Kite, E. S., Fassett, C. I. & Guzewich, S. D. Limits on runoff episode duration for early Mars: integrating lake hydrology and climate models. *Geophys. Res. Lett.* **48**, 10 (2021).
57. Ramirez, R. M., Craddock, R. A. & Usui, T. Climate simulations of early Mars with estimated precipitation, runoff, and erosion rates. *J. Geophys. Res. Planets* **125**, e2019JE006160 (2020).
58. Price, J. R., Velbel, M. A. & Patino, L. C. Rates and time scales of clay-mineral formation by weathering in saprolitic regoliths of the southern Appalachians from geochemical mass balance. *Geol. Soc. Am. Bull.* **117**, 783–794 (2005).
59. Schmidt, P. W., Prasad, V. & Ramam, P. K. Magnetic ages of some Indian laterites. *Palaeogeography, Palaeoclimatology, Palaeoecology* **44**, 185–202 (1983).
60. Retallack, G. J., Bestland, E. A. & Fremd, T. J. *Eocene and Oligocene Paleosols of Central Oregon*. Vol. 344 (Geological Society of America, 1999).
61. Wolff-Boenisch, D., Gislason, S. R., Oelkers, E. H. & Putnis, C. V. The dissolution rates of natural glasses as a function of their composition at pH 4 and 10.6, and temperatures from 25 to 74 C. *Geochim. Cosmochim. Acta* **68**, 4843–4858 (2004).
62. Stopar, J. D., Jeffrey Taylor, G., Hamilton, V. E. & Browning, L. Kinetic model of olivine dissolution and extent of aqueous alteration on mars. *Geochim. Cosmochim. Acta* **70**, 6136–6152 (2006).
63. Olsen, A. A. & Rimstidt, J. D. Using a mineral lifetime diagram to evaluate the persistence of olivine on Mars. *Am. Miner.* **92**, 598–602 (2007).
64. Williams, R. M. & Weitz, C. M. Reconstructing the aqueous history within the southwestern Melas basin, Mars: clues from stratigraphic and morphometric analyses of fans. *Icarus* **242**, 19–37 (2014).
65. Irwin, R. P. III, Lewis, K. W., Howard, A. D. & Grant, J. A. Paleohydrology of Eberswalde crater, Mars. *Geomorphology* **240**, 83–101 (2015).
66. Palucis, M. C. et al. Sequence and relative timing of large lakes in Gale crater (Mars) after the formation of Mount Sharp. *J. Geophys. Res.: Planets* **121**, 472–496 (2016).
67. Kite, E. S., Sneed, J., Mayer, D. P. & Wilson, S. A. Persistent or repeated surface habitability on Mars during the late Hesperian-Amazonian. *Geophys. Res. Lett.* **44**, 3991–3999 (2017).
68. Grotzinger, J. P. et al. Deposition, exhumation, and paleoclimate of an ancient lake deposit, Gale crater, Mars. *Science* **350**, aac7575 (2015).
69. Segura, T. L., Toon, O. B., Colaprete, A. & Zahnle, K. Environmental effects of large impacts on Mars. *Science* **298**, 1977–1980 (2002).
70. Johnson, S. S., Pavlov, A. A. & Mischna, M. A. Fate of SO_2 in the ancient Martian atmosphere: implications for transient greenhouse warming. *J. Geophys. Res. Planets* **114**, E11 (2009).
71. White, A. F. & Brantley, S. L. The effect of time on the weathering of silicate minerals: why do weathering rates differ in the laboratory and field? *Chem. Geol.* **202**, 479–506 (2003).
72. Schultz, P. H. & Mustard, J. F. Impact melts and glasses on Mars. *J. Geophys. Res. Planets* **109**, E1 (2004).
73. Michalski, J. R. & Bleacher, J. E. Supervolcanoes within an ancient volcanic province in Arabia Terra, Mars. *Nature* **502**, 47–52 (2013).
74. Huang, J. & Xiao, L. Knobby terrain on ancient volcanoes as an indication of dominant early explosive volcanism on Mars. *Geophys. Res. Lett.* **41**, 7019–7024 (2014).
75. Parfitt, R. Allophane and imogolite: role in soil biogeochemical processes. *Clay Minerals* **44**, 135–155 (2009).
76. Rasmussen, C., Dahlgren, R. A. & Southard, R. J. Basalt weathering and pedogenesis across an environmental gradient in the southern Cascade Range, California, USA. *Geoderma* **154**, 473–485 (2010).
77. Whelley, P. et al. Stratigraphic evidence for early martian explosive volcanism in Arabia Terra. *Geophys. Res. Lett.* **48**, e2021GL094109 (2021).
78. Ehlmann, B. L. & Buz, J. Mineralogy and fluvial history of the watersheds of Gale, Knobel, and Sharp craters: a regional context for the Mars Science Laboratory Curiosity's exploration. *Geophys. Res. Lett.* **42**, 264–273 (2015).
79. Zolotov, M. Y. & Mironenko, M. V. Chemical models for martian weathering profiles: insights into formation of layered phyllosilicate and sulfate deposits. *Icarus* **275**, 203–220 (2016).
80. Du, P. et al. Structure of allophanes with varied Si/Al molar ratios and implications to their differentiation on Mars. *Icarus* **382**, 115057 (2022).
81. Bultel, B., Viennet, J. C., Poulet, F., Carter, J. & Werner, S. C. Detection of carbonates in Martian weathering profiles. *J. Geophys. Res. Planets* **124**, 989–1007 (2019).
82. Howard, A. D. & Moore, J. M. The light-toned sediments in and near lower Mawrth Vallis may be a drape deposit. *38th Lunar and Planetary Science Conference (Lunar and Planetary Science XXXVIII)*, held March 12–16, 2007 in League City, Texas. LPI Contribution Abstract No. 1338, p. 1339 (2007).
83. Howard, A. D., Moore, J. M. & Irwin III, R. P. An intense terminal epoch of widespread fluvial activity on early Mars: 1. Valley network incision and associated deposits. *J. Geophys. Res. Planets* **110**, E12 (2005).
84. Irwin, R. P., Howard, A. D., Craddock, R. A. & Moore, J. M. An intense terminal epoch of widespread fluvial activity on early Mars: 2. Increased runoff and paleolake development. *J. Geophys. Res. Planets* **110**, E12 (2005).
85. Fassett, C. I. & Head, J. W. Sequence and timing of conditions on early Mars. *Icarus* **211**, 1204–1214 (2011).
86. Michalski, J. R. et al. Geological diversity and microbiological potential of lakes on Mars. *Nat Astron* **6**, 1133–1141 (2022).
87. Dickson, J. L., Kerber, L. A., Fassett, C. I. & Ehlmann, B. L. A global, blended CTX mosaic of Mars with vectorized seam mapping: a new mosaicking pipeline using principles of non-destructive image editing. In *Lunar and Planetary Science Conference* Vol. 49, pp. 1–2 (Lunar and Planetary Institute, The Woodlands, TX, USA, 2018).
88. McEwen, A. S. et al. Mars reconnaissance orbiter's high resolution imaging science experiment (HiRISE). *J. Geophys. Res. Planets* **112**, E5 (2007).
89. Edwards, C. S., Christensen, P. R. & Hill, J. Mosaicking of global planetary image datasets: 2. Modeling of wind streak thicknesses observed in Thermal Emission Imaging System (THEMIS) daytime and nighttime infrared data. *J. Geophys. Res.* **116**, https://doi.org/10.1029/2011je003857 (2011).
90. Ivanov, B. A. Mars/Moon cratering rate ratio estimates. *Space Sci. Rev.* **96**, 87–104 (2001).
91. Werner, S. C. & Tanaka, K. L. Redefinition of the crater-density and absolute-age boundaries for the chronostratigraphic system of Mars. *Icarus* **215**, 603–607 (2011).
92. Beyer, R. A., Alexandrov, O. & McMichael, S. The Ames Stereo Pipeline: NASA's open source software for deriving and processing terrain data. *Earth Space Sci.* **5**, 537–548 (2018).
93. Hartmann, W. K. & Neukum, G. Cratering chronology and the evolution of Mars. In Chronology and Evolution of Mars. Space Sciences Series of ISSI Vol. 12 (eds Kallenbach, R., Geiss, J., Hartmann, W. K.) (Springer, Dordrecht) https://doi.org/10.1007/978-94-017-1035-0_6 (2001).
94. Kneissl, T., van Gasselt, S. & Neukum, G. Map-projection-independent crater size-frequency determination in GIS environments—new software tool for ArcGIS. *Planet Space Sci.* **59**, 1243–1254 (2011).
95. Warner, N. H. et al. Minimum effective area for high resolution crater counting of martian terrains. *Icarus* **245**, 198–240 (2015).
96. Robbins, S. J. et al. Revised recommended methods for analyzing crater size-frequency distributions. *Meteorit. Planet. Sci.* **53**, 891–931 (2018).
97. Palucis, M. C., Jasper, J., Garczynski, B. & Dietrich, W. E. Quantitative assessment of uncertainties in modeled crater retention ages on Mars. *Icarus* **341**, 113623 (2020).
98. Irwin, R. P., Tanaka, K. L. & Robbins, S. J. Distribution of early, middle, and late Noachian cratered surfaces in the Martian highlands: implications for resurfacing events and processes. *J. Geophys. Res. Planets* **118**, 278–291 (2013).
99. Jay, A. E. & Widdowson, M. Stratigraphy, structure and volcanology of the SE Deccan continental flood basalt province: implications for eruptive extent and volumes. *J. Geol. Soc.* **165**, 177–188 (2008).
100. Van de Graaff, W. E. Relict early Cainozoic drainages in arid Western Australia. *Zeitschrift fur Geomorphologie* **21**, 379–400 (1977).
101. McSween Jr, H. Y. Petrology on mars. *Am. Miner.* **100**, 2380–2395 (2015).
102. Batalha, N. E., Kopparapu, R. K., Haqq-Misra, J. & Kasting, J. F. Climate cycling on early Mars caused by the carbonate–silicate cycle. *Earth Planetary Sci. Lett.* **455**, 7–13 (2016).

Acknowledgements

This work was funded by the Hong Kong Research Grants Council General Research Fund to J.R.M. (17301718) and the Canadian Institute for Advanced Research (CIFAR) Earth 4-D Program.

Author contributions

B.Y. carried out all data analyses and wrote the original manuscript. J.M. conceptualized the project and edited the paper.

Competing interests

The authors declare no competing interests.

Additional information

Supplementary information The online version contains supplementary material available at https://doi.org/10.1038/s43247-022-00602-7.

Correspondence and requests for materials should be addressed to Joseph R. Michalski.

Peer review information *Communications Earth & Environment* thanks Janice Bishop and the other, anonymous, reviewer(s) for their contribution to the peer review of this work. Primary Handling Editors: Claire Nichols, Joe Aslin, Heike Langenberg.